Ibn Al-Haitham Journal for Pure and Applied Sciences
Journal homepage: jih.uobaghdad.edu.iq
PISSN: 1609-4042, EISSN: 2521-3407
IHJPAS. 2025, 38 (1)

Studying the Change in the Dislocation Density and the Burger Vector when the Temperature Changes Using the Method of Analysis X-Ray Diffraction Patterns

Maysaa A. Hameed[1*], Khalid H. Harbbi[2]
[1,2]Department of Physics, College of Education for Pure Sciences (Ibn Al-Haitham), University of Baghdad, Baghdad, Iraq.
[*]Corresponding Author.

Received:13 March 2024 Accepted: 22 May 2024 Published: 20 January 2025
doi.org/00.000000.000000

Abstract

The current study investigated ways temperature affects the structural and Material features of ZnO. The temperature varied between 300,500 and 700°C. Zinc oxide's physical characteristics were determined using diffraction of x-rays. The patterns of x-ray diffraction revealed the excellent purity, crystalline, and nanoscale nature of the ZnO nanoparticles. size was found and computed using the Halder-Wagner method, in that order. As the temperature of annealing rises, the size of the crystallite grew. Therefore, it was found that the annealing temperature greatly affects structural and morphological characteristics. The specimen was examined to compute physical and microstructural characteristics like lattice strain, dislocation density, additionally burger vector, Results for the dislocation density and Burger vector obtained for 300 °C are ($43.7832 * 10^{-5}$ $(1/nm)^2$, $3.576 * 10^{-1}$), for 500°C are ($30.6388 * 10^{-5}$ $(1/nm^2)$,$5.3688* 10^{-1}$) and for 700°C are. ($18.2516* 10^{-5}$ $(1/nm^2)$,$6.263*10^{-1}$).

Keywords: X-ray diffraction, lattice strain, crystallite size, Burger vector.

1. Introduction

An increasingly popular method for testing materials is X-ray diffraction (XRD). To determine the material's composition, including crystalline size, strain, stress, density, and energy, diffraction data was used. The size of the crystallite is used to measure coherent diffracting patterns. The size of a particle's crystallite does not always match its size because of polycrystalline. Separating and differentiating broadening caused by measurements and causes from broadening caused by crystallite size can be quite difficult. There will always be errors, can produce more accurate data by reducing the errors in the greatest method feasible. A particle contains several nanoscale or microscale crystals, making it impossible to calculate the size of the nanoparticles collected from XRD patterns. Since information can be obtained by an X-ray passing through the crystal, the size computation is related to the crystals rather than the particles (1-3). The atoms' orderly arrangement

inside the crystal lattice causes both beneficial and harmful interference for monochromatic radiation when they collide with the materials of crystalline. A diffraction pattern is produced by the interference and is captured by a detector. then applied to determine the fundamental specifics of the specimen(3,4). Bragg's law, n λ = 2d sin θ, applies to when-prepared and annealed nanoparticle sample diffraction. Here, n is an integer number, λ is the wavelength of radiation is the distance between planes, and θ is the angle of diffraction (5,6). Small crystallite size and internal lattice deformation both lead to the x-ray diffraction peaks' widening. Techniques have evolved throughout the previous decade or so to distinguish between those two basic impacts and further consequences such as twin or planar defects(7). Some techniques for measuring materials include the strain-size plot, Williamson-Hall (W-H), Scherrer, and Halder-Wagner (H-W) techniques, the approach of Williamson-Hall uses the diffraction peak's FWHM values, whereas the Scherrer method employs full-width half-maximum (FWHM) to calculate the size of the crystals. is a properly easy and suitable one for calculating average size as well as determining various elastic properties, such as strain. The Halder-Wagner technique, conversely, uses an assumption that the peak's physical expansion is a function of Voigt and additionally calculates the mean dimensions and stress using the XRD data peak expansion(8-15). This work deals with a comparison of the values of the crystalline size of ZnO nanoparticles calculated by the Halder-Wagner method and some of the physical parameters relied upon in the calculation, that were not previously calculated, such as the dislocation density and the Burger vector at high temperature using X-ray diffraction.

2. Materials and Methods

2.1. Halder-Wagner Method

The SSP approach assumes a Gaussian function for strain increasing and a Lorentzian function for expansion of the XRD peak profile in size. However, in reality, The XRD peak does not follow a Gaussian or Lorentzian function. since the XRD peak region corresponds nicely to the Gaussian function, However, its tail drops too fast to match. In contrast, The tails of the profile match the Lorentz function. rather well, nevertheless, they don't line up with the XRD peak zone. , since the Broadening of the peak is a convolution of the Lorentzian collaboration, therefore, a symmetric Voigt function, the Wagner-Halder method is applied to get around this problem. Thus, employing the Halder-Wagner Technique, the entire breadth of the physical profile at its maximal half-width may be expressed for the function of Voigt(16- 18). The Halder-Wagner method provides the link between the lattice strain and the crystalline size.:

$$(\beta_{hkl} / d_{hkl})^2 = (1/D). (\beta_{hkl} / d^2_{hkl}) + (\xi/2)^2 \quad (1)$$

The straight line equation above is now generating a graph of $(\beta_{hkl} / d_{hkl})^2$ vs (β_{hkl}/d^2_{hkl}), where (β_{hkl} /d^2_{hkl})represents the horizontal axis X and a $(\beta_{hkl}/d_{hkl})^2$ represents the vertical axis Y (19,20). where The integral width is represented by β and Lattice plane spacing is denoted by d. Let D be the size of the crystallites and ξ be a measure of lattice strain (21,22). It should be mentioned that different theories involving How to use X-ray diffraction data to calculate the size of crystallite have been put forward in the past. The Halder-Wagner approach described here is one of them by:

$$(\beta/\tan\theta)^2 = (k\lambda/D). (\beta / \tan\theta \sin\theta) + 16\,\xi^2 \quad (2)$$

Whereas D and ξ stand for the size and strain of the Halder-Wagner crystallites, respectively, The form factor is K equal to (0.89) and The symbol λ is used to represent the radiation wavelength

in the manometer (0.15405nm). To compute the crystallite size (D), the lattice strain (ξ) utilizing the formulas :

$$D = K\lambda / \text{slope} \quad (3)$$

$$\xi = (\text{intercept}/16)^{1/2} \quad (4)$$

and to determine dislocation density (ρ) and Burger vector(b) using the equations:

$$\rho = 1/D^2 \quad (1/nm^2) \quad (5)$$

$$b = (14.4\ \xi^2/\rho)^{1/2} \quad (6)(23\text{-}27).$$

2.2. Integral Breadth Method

With the method of integral breadth, which is a one-line technique, Presumably, the strain and size related to expansion caused by average crystal size (areas of coherent dispersion) and lattice strains (often referred to as lattice defects) caused by, for example, the presence of lattice defects can be represented as the Cauchy and Gaussian (Lorentzian) Voigt's integral breadth. The integral width could be utilized for calculations of the effects of the size of particles and strain when using it as a measure of the peak profile:

Integral Breadth (β)= Peak Area/Intensity Maxima (7) (28,29).

Typically, the diffraction data is represented by the angle (2θ) distribution. The greatest peak intensity (Imax) and integrated intensity I (the region beneath the peak) were computed following background subtraction. The location of the peak can be determined in several ways. Peak width can usually be computed using the full width at half maximum intensity (FWHM) connected to the biggest peak width at half maximum intensity, or the integrated width on a rectangular screen with the same higher and integrated intensity while the observed peak. distinct peak variables are utilized based on the objective of the observations (30). The theoretical basis for the relationship between annealing temperature and structural properties is explained in(31).

3. Results and Discussions

The ZnO powder was purchased with a purity of 99.9%, and 10 grams were burned at each temperature, after examination with an XR diffractometer The x-ray diffraction patterns showed several peaks that matched unique ZnO planes after calcination. where The temperatures at which the specimens were burnt varied from 300, 400, and 700°C. Cu-k diffractometers made in Japan, the SHIMADZU model (6000), was used to obtain intensity data on ZnO nanoparticles for each of the seven peaks, as shown in **Figures 1, 2,** and **3.** A program for analysis named Origin Pro Lab is used to develop the peak outline using this data. The integral width is computed after the program computes the FWHM and area under the curve. The same procedures were followed for the surfaces (100), (002), (101), (102), (110), (103), (112).

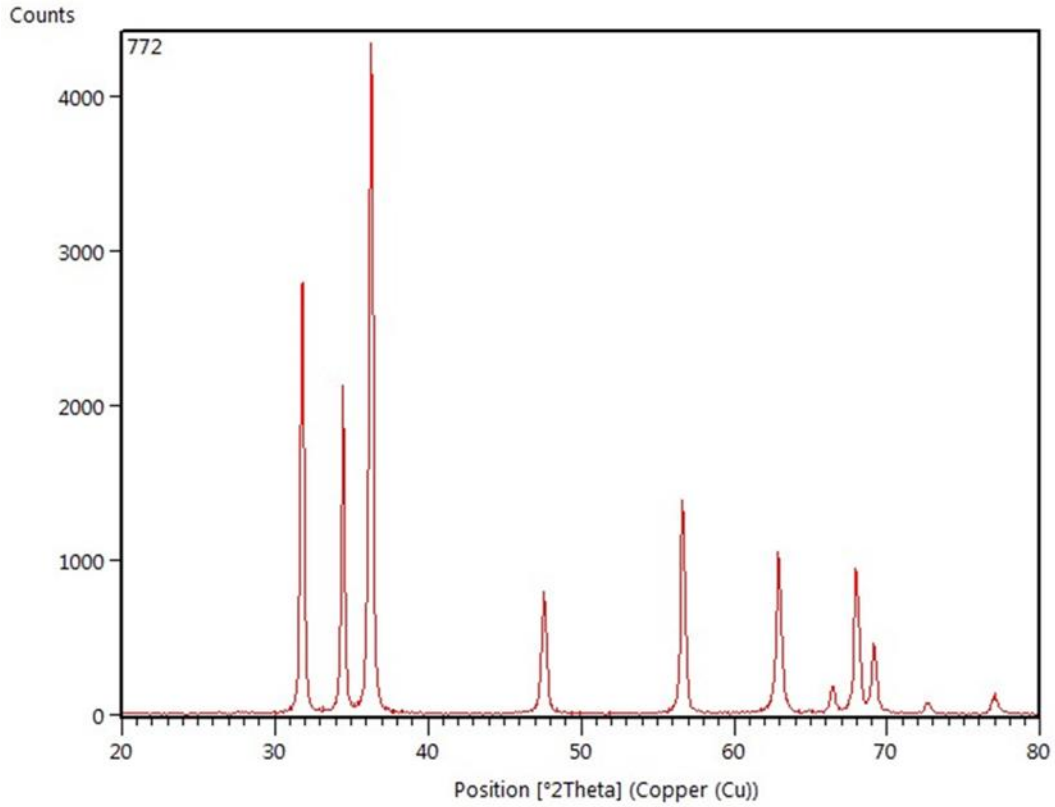

Figure1. XRD pattren of ZnO at 300°C.

Regarding the values of (hkl) for **Figures 1- 3.** , the values of (hkl) are (100), (002), (101), (102),(110),(103),(112) and the corresponding angles (31.766)°,(34.419)°,(36.251) °,(47.536)°, (56.591)°,(62.852)°,(67.942)° are constant for all figures, but there is a change in the intensity values calculated for the three figures, which was taken into account in the calculations.

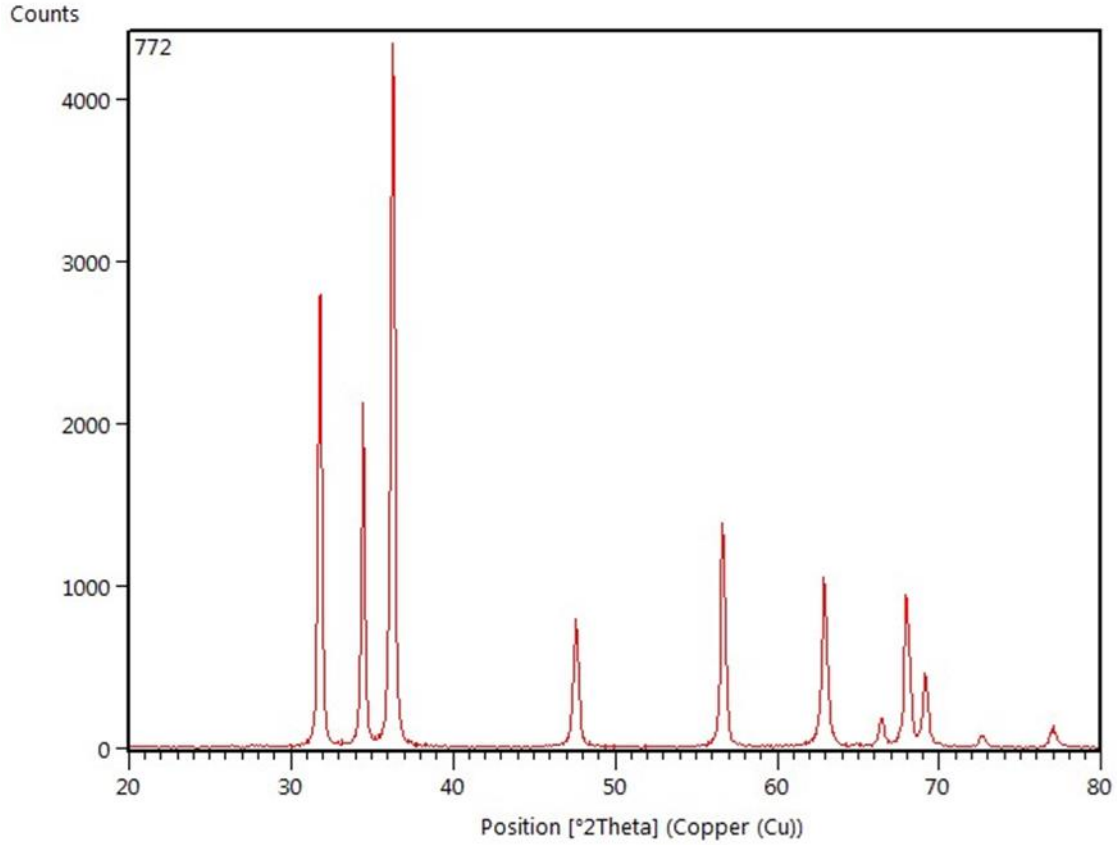

Figure2. XRD pattren of ZnO at 500°C.

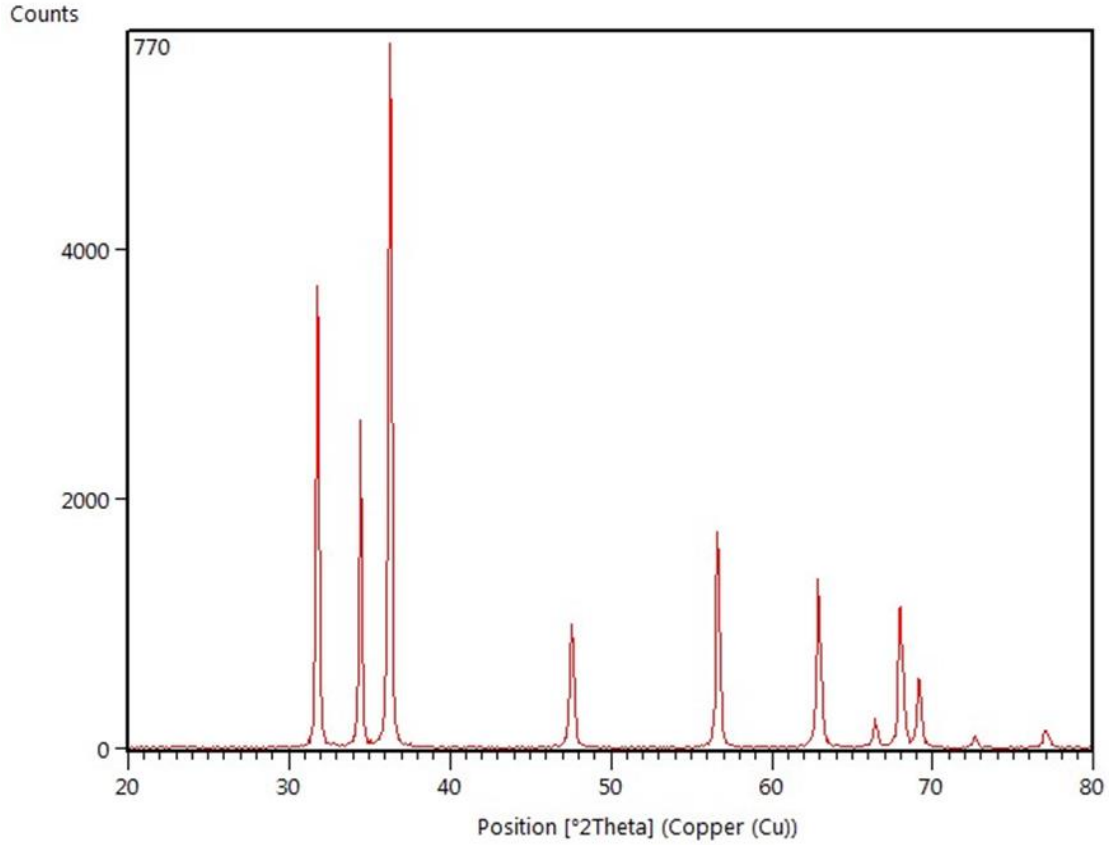

Figure3. XRD pattren of ZnO at 700°C.

3.1 The Halder-Wagner Method:

The form of the peaks in ZnO was examined using an analytical instrument known as Origin Pro Lap, Subsequently, each of the peaks in the shape had fittings to obtain the peak's pure line. , we will take one of the diffraction lines of x- radiation, which is (002) at 300 °C, 500 °C, and 700 °C, as a model for analysis (XRD) diffraction, shown in **Figure 4,** and the same steps will be taken to analyze all the other lines at the mentioned temperatures**.**

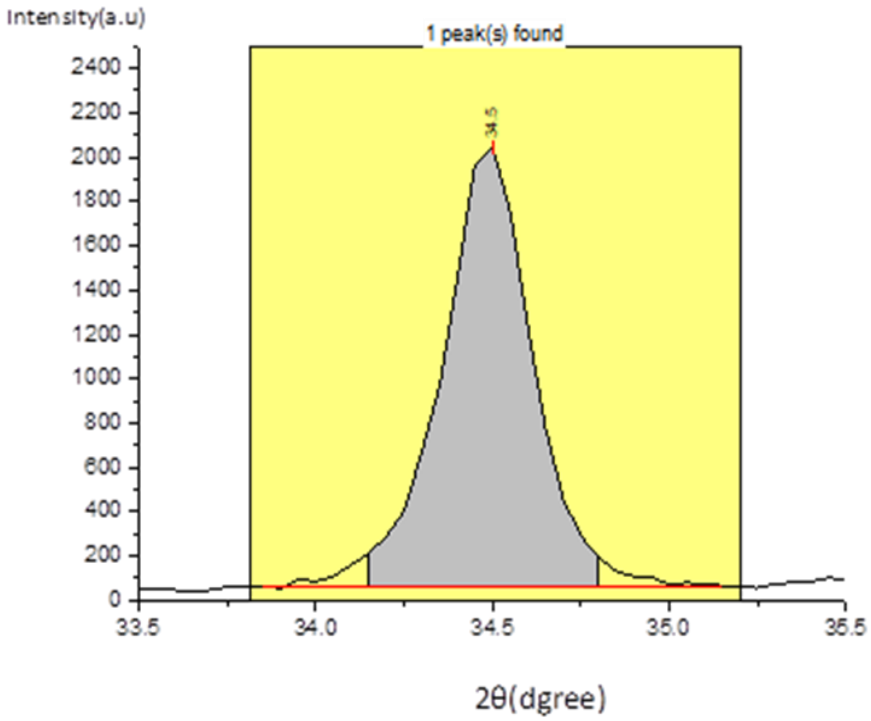

Figure 4. The Peak(002) Fit of ZnO nanoparticle.

To obtain the most precise and pure line for each peak in the pattern, 40 steps were taken on the peak's fitting line in addition to the high-intensity step for each peak after the peaks were fitted as shown in **Figure 5.**

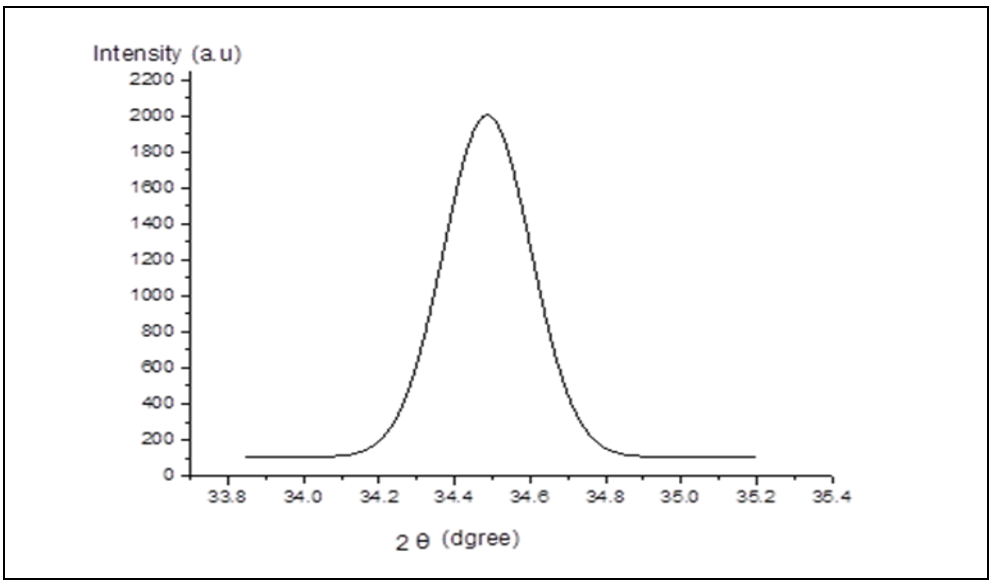

Figure 5. After fitting for 40 steps for peak (002) of ZnO.

Following the subtraction of intensity to obtain clear Values of background for every peak, the area under the curve was computed. The integral of the breadth for each peak was then calculated after estimating the full width at a half-maximum derived from the formula ($B=A/I_{\circ}$), whereas A is the peak's area under the curve and $I_{\circ}$ is the peak's maximum intensity. shown in **Figure 6**, the result of full width at a half maximum and the integral breadth (IB) for the peak (002) shown in **Table 1**.

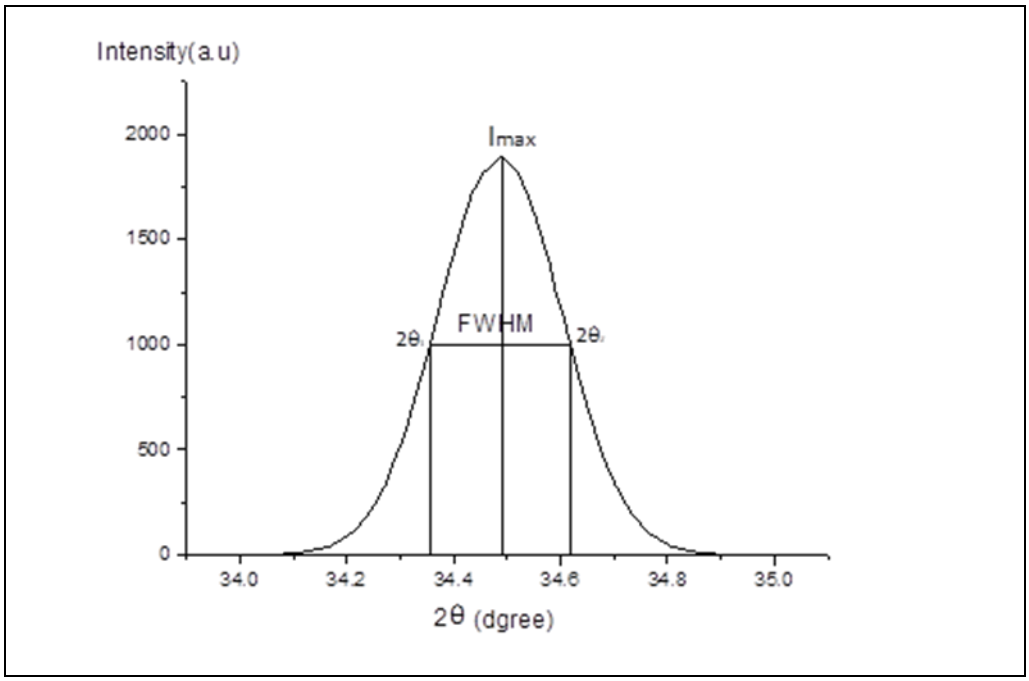

Figure 6. Identified the full width at half maxima of the peak (002) of ZnO.

Table1. Estimated the high intensity, the region beneath the curve, (FWHM), and the integral breadth.

hkl	Intensity($I_{\circ}$)	Area under the curve (A)	(FWHM)	$\beta = A/I_{\circ}$
(002)	2003.1875	658.6443006	0.2674	0.328798128

After that calculate the values of ($\beta/(\tan\theta \sin\theta)$) and $(\beta/\tan\theta)^2$ for the temperature (300,500,700) °C listed in **Tables 2- 4.** We plot a graph with the horizontal axis X representing ($\beta/\tan\theta \sin\theta$) and the vertical axis Y representing $(\beta/\tan\theta)^2$ appeared in **Figures 6-8.**

Table 2. The calculation used for (H.W) plot at 300°C.

(hkl)	2θ(degree)	θ(rad.)	tan θ	Sin θ	FWHM*(π/180)	β/(tan θ sin θ)	(β/ tan θ)²
(100)	31.8364	0.277684156	0.285048654	0.274129255	0.004430889	0.056704363	0.000241626
(002)	34.4831	0.300769261	0.310179321	0.296255022	0.004341922	0.047250181	0.000195947
(101)	35.8871	0.313015261	0.323655386	0.30792878	0.003952911	0.039662851	0.000149166
(102)	36.311	0.316712611	0.327744956	0.311444361	0.004830367	0.047322057	0.000217214
(110)	47.5937	0.415122828	0.440735401	0.403302329	0.005606644	0.031542372	0.000161827
(103)	56.6398	0.494024922	0.538569322	0.474173388	0.0049769	0.019488577	8.53954E-05
(112)	63.2733	0.551883783	0.615700107	0.524292272	0.002508511	0.007770936	1.65994E-05

Table 3. The calculation used for (H.W) plot at 500°C.

hkl	2θ(degree)	θ(rad.)	tan θ	sin θ	FWHM*(π/180)	β/(tan θ sin θ)	(β/ tan θ)²
(100)	31.7858	0.277242811	0.284571509	0.27370479	0.004504156	0.057828186	0.000250521
(002)	34.4291	0.300298261	0.309663081	0.295805133	0.0043803	0.047819906	0.000200092
(101)	35.7372	0.3117078	0.322211574	0.306684586	0.004971667	0.050311691	0.000238079
(102)	36.2621	0.316286094	0.32727269	0.311039029	0.004922822	0.048360357	0.000226261
(110)	47.5444	0.414692822	0.440221965	0.402908808	0.005829933	0.032868896	0.000175381
(103)	56.5967	0.493648994	0.538084452	0.473842375	0.004891422	0.019184514	8.2636E-05
(112)	63.1733	0.551011561	0.614497882	0.523549342	0.0031714	0.009857641	2.66355E-05

Table 4. The calculation used for (H.W) plot at 700°C.

(hkl)	2θ(degree)	θ(rad.)	tan θ	sin θ	FWHM*(π/180)	β/(tan θ sin θ)	(β/ tan θ)²
(100)	31.8285	0.27761525	0.284974151	0.274062988	0.003890111	0.049808808	0.000186343
(002)	34.4784	0.300728267	0.310134383	0.296215868	0.003891856	0.042364148	0.000157476
(101)	36.3099	0.316703017	0.327734331	0.311435243	0.004136078	0.040522759	0.00015927
(102)	36.6864	0.319986933	0.331374904	0.314554157	0.004280867	0.041069239	0.000166888
(110)	47.586	0.415055667	0.440655197	0.403240871	0.004556489	0.025642884	0.000106921
(103)	56.6409	0.494034517	0.5385817	0.474181835	0.003945933	0.015450881	5.3678E-05
(112)	66.4151	0.579287261	0.654150245	0.547427618	0.004322733	0.012071305	4.36679E-05

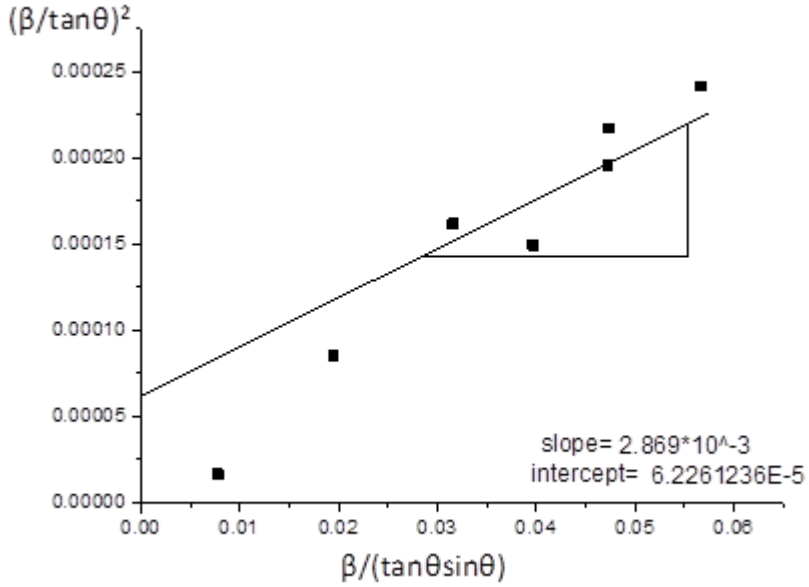

Figure 6. Plot of connection (β/tan θ) with (β/tan θ sin θ) at 300 °C.

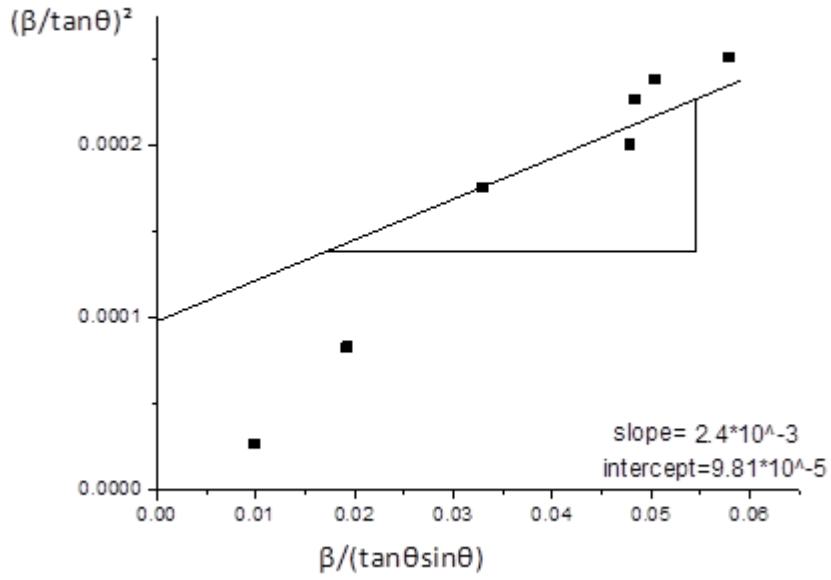

Figure 7. Plot of connection (β /tan θ) with (β /tan θ sin θ) at 500 °C.

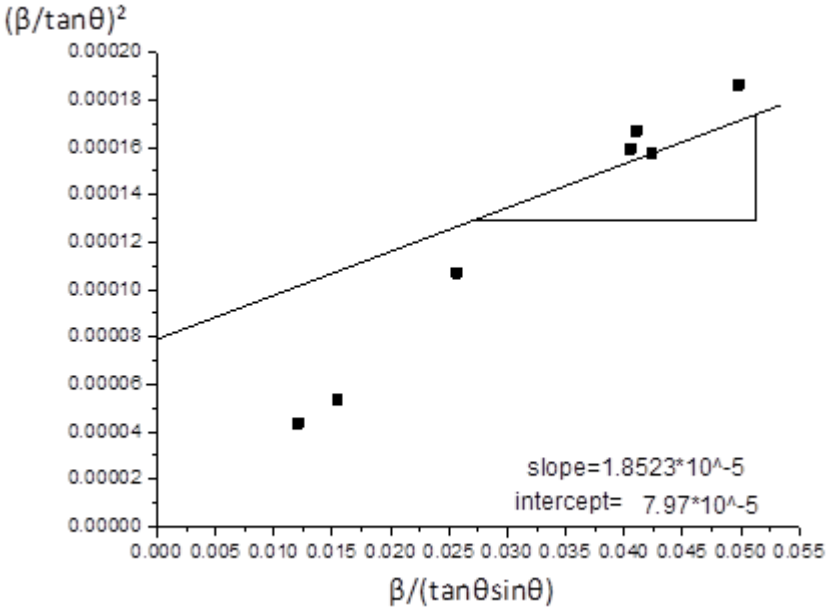

Figure 8. Plot of connection (β/ tan θ) with (β /tan θ sin θ) at 700 °C.

This helps us to determine the plot's slope and intercept, Starting from a slope of the graph line the size of the crystal was calculated, and based on the intercept, the lattice strain was calculated using equations (3) and (4). Then the dislocation density and Burger vector were calculated through equations (5) and (6), for all temperatures, and the results were listed in **Table 4**.

Table 4. Estimating crystallite size, lattice strain, dislocation density, and Burger vector for Halder-Wagner method at (300,500,700) °C.

T(°C)	D (nm)	ξ	ρ(1/nm^2)	b
300	47.791	$1.972*10^{-3}$	$43.7832 * 10^{-5}$	$3.576 * 10^{-1}$
500	57.13	$2.476*10^{-3}$	$30.6388 * 10^{-5}$	$5.368* 10^{-1}$
700	74.02	$2.23*10^{-3}$	$18.2516 * 10^{-5}$	$6.263* 10^{-1}$

4. Conclusion:

The previous table makes it evident that values of crystallite size D rise as temperature rises, which makes sense given that x-ray intensity increases as temperature rises from 300 to 700 °C. A strong correlation exists between the value of crystallite size and the full width at half maximum (FWHM). A decrease in the dislocation density ξ value was observed, by the laws established in this piece of writing, as the size of the grains grew. As the temperature increased, an increase in Burger vector b values was seen because of the inverse proportionality between the dislocation density and the Burger vector. As the temperature increases (300,500,700)°C, an expansion occurs in the sample size, and this means an increase in the grain size, which is shown in Table(4), where the values of the grain size (47.791, 57.13, 74.02) were for the temperatures (300,500,700)°C, respectively. Based on the grain size values, the dislocation density was calculated, considering the inverse proportionality Between the dislocation density and the grain size, the results were consistent, as listed in the previous table. The Burger vector for the three temperatures (300,500,700) °C was calculated based on the strain values calculated from the three Figures (6,7,8), and the results of the Burger vector for the three temperatures (300,500,700) °C were as shown($3.576 * 10^{-1}$, $5.368* 10^{-1}$, $6.263* 10^{-1}$) respectively.

Acknowledgment

I am grateful to the College of Education for Pure Science, Ibn Al-Haitham, and the University of Baghdad for their cooperation in finishing This investigation. The Physics Department personnel opened private laboratories and provided scientific facilities to help support the research effort.

Conflict of Interest

The authors declare that they have no conflicts of interest.

Funding

None.

Ethical Clearance

The Ministry of Health and Environment of Iraq issued the directions for the work done in the laboratories.

References

1. Jaleel MT, Harbbi KH. Study of the x-ray diffraction lines of calcium titanate nanoparticle using SSP method and Scherrer method . AIP Conf Proc. 2023;2769(1): 45-56. https://doi.org/10.1063/5.0129557.
2. Rabiei M, Palevicius A, Monshi A, Nasiri S, Vilkauskas A, Janusas G. Comparing methods for calculating nanocrystal size of natural hydroxyapatite using X-ray diffraction. Nanomaterials. 2020;10(9): 23-34. http://dx.doi.org/10.3390/nano10091627.
3. Sami AM, Harbbi KH. Analysis the average lattice strain in the crystal direction (hkl) in MgO nanoparticles by using modified Williamson-Hall method. AIP Conf Proc. 2022; 2394(1): 12-24. https://doi.org/10.1063/5.0122941.
4. Surdu VA, Győrgy R. X-ray diffraction data analysis by machine learning methods-a review. Appl. Sci. .2023;13(17): 9992. https://doi.org/10.3390/app13179992.
5. Mongkolsuttirat K, Buajarern J. Uncertainty evaluation of crystallite size measurements of nanoparticle using X-ray diffraction analysis (XRD). J Phys Conf Ser. 2021; 1719(1):012054. https://doi:10.1088/1742-6596/1719/1/012054.
6. Wilhelm M, Lotter F, Scherdel C, Schmitt J. Advancing Efficiency in Mineral Construction Materials Recycling: A Comprehensive Approach Integrating Machine Learning and X-ray Diffraction Analysis. Buildings. 2024;14(2):340. https://doi.org/10.3390/buildings14020340.
7. Yogamalar R, Srinivasan R, Vinu A, Ariga K, Bose AC. X-ray peak broadening analysis in ZnO nanoparticles. Solid State Commun. 2009;149(43-44):1919 -1923. https://doi:10.1016/j.ssc. 2009.07.043.
8. Deb AK, Chatterjee P. Estimation of lattice strain in alumina-zirconia nanocomposites by X-ray diffraction peak profile analysis. J Theor Appl Phys. 2019;13:(221–229). https://doi.org/10.1007/s40094-019-0338-z.
9. Kushwaha P, Chauhan P. Microstructural evaluation of iron oxide nanoparticles at different calcination temperatures by Scherrer, Williamson-Hall, Size-Strain Plot and Halder-Wagner methods. phase transitions. 2021;94,(10):731-753. https://doi.org/10.1080/01411594.2021.1969396.
10. Sen SK, Barman UC, Manir MS, Mondal P, Dutta S, Paul M, Hakim MA. X-ray peak profile analysis of pure and Dy-doped α-MoO3 nanobelts using Debye-Scherrer, Williamson-Hall and Halder-Wagner methods. Adv Nat Sci. Nanosci. Nanotechnol. 2020;11(2): 025004. https://doi.org/10.1088/2043-6254/ab8732
11. Gholizadeh A, Malekzadeh A, Ghiasi M. Structural and magnetic features of LaO. 7SrO. 3Mn1−xCoxO3 nano-catalysts for ethane combustion and CO oxidation. Ceram Int. 2016;42(5): 5707-5717. https://doi.org/10.1016/j.ceramint.2015.12.101.
12. Sitdikov VD, Chizhov PS, Murashkin MY, Goidenko AA, Valie RZ. X-ray studies of dynamic aging in an aluminum alloy subjected to severe plastic deformation. Mater Charact. 2015;110:222-227. https://doi.org/10.1016/j.matchar.2015.10.037.
13. Ravidhas C, Josephine AJ, Sudhagar P, Devadoss A, Terashima C, Nakata K, Sanjeeviraja C. Facile synthesis of nanostructured monoclinic bismuth vanadate by a co-precipitation method: Structural, optical and photocatalytic properties. Mater Sci. Semicond. Process. 2015;30:343-351. https://doi.org/10.1016/j.mssp.2014.10.026.
14. Gopinath S, Philip J. Preparation of metal oxide nanoparticles of different sizes and morphologies their characterization using small angle X-ray scattering and study of thermal properties. Mater Chem Phys. 2014;145(1-2):213-221. https://doi.org/10.1016/j.matchemphys.2014. 02.005.
15. Gholizadeh A, Jafari E. Effects of sintering atmosphere and temperature on structural and magnetic properties of Ni-Cu-Zn ferrite nano-particles: Magnetic enhancement by a reducing atmosphere. J. Magn Magn Mater. 2017;422:328-336. https://doi.org/10.1016/j.jmmm.2016.09.029.
16. Nath D, Singh F, Das R. X-ray diffraction analysis by Williamson Hall, Halder-Wagner and size-strain plot methods of CdSe nanoparticles-a comparative study. Mater Chem Phys. 2020;239:122021. https://doi.org/10.1016/j.matchemphys.2019.122021.

17. Jahil SS, Mohammed IA, Khazaal AR, Jasim KA, Harbbi KH. Application the Halder–Wagner to Calculation Crystal Size and Micro Strain by X-ray Diffraction Peaks Analysis. NeuroQuantology. 2022;20(1):199-204. https://doi:10.14704/nq.2022.20.1.NQ22074.
18. Al-Shomar SM, Akl AA, Mansour D, Hedhili F, Aslam A, Shaaban ER, Mahmoud SA. Influence of Mo_{+2} ion concentration on crystallization, microstructure, crystal imperfection and morphology of WO_3 sprayed thin films. Mater Res Express. 2022;9(9):096404. https://DOI:10.1088/2053-1591/ac9273.
19. Kamil MK, Jasim KA. Calculating of crystalline size, strain, and Degree of crystallinity of the compound ($HgBa_2Ca_2Cu_3O_{8+\sigma}$) by different method. IOP Conf Ser Mater Sci Eng. 2020;928(7):072109. https://DOI.10.1088/1757-899X/928/7/072109.
20. Harbbi KH. Effect of the Synthesis Time on Structural Properties of Copper Oxide. Ibn AL-Haitham J Pure Appl Sci. 2023;36(2):181-190. https://doi.org/10.30526/36.2.3024.
21. Harbbi KH. The Effect of Annealing Temperatures on Structural Properties of Cu_2O Nanoparticles. Ibn Al-Haitham J Pure Appl Sci. 2023;36(3):148-157. https://doi.org/10.30526/36.3.3116.
22. Disha SA, Hossain MS, Habib ML, Ahmed S. Calculation of crystallite sizes of pure and metals doped hydroxyapatite engaging Scherrer method, Halder-Wagner method, Williamson-Hall model, and size-strain plot. Results Mater. 2024;21:100496. https://doi.org/10.1016/j.rinma.2023.100496.
23. Izumi F, Ikeda T. Implementation of the Williamson-Hall and Halder-Wagner methods into RIETAN-FP. Doctoral dissertation, Nagoya Institute of Technology. 2015;3:33-38. http://doi.id.nii.ac.jp/1476/00002383/.
24. Jalil MT, Harbbi KH. Using the Size Strain Plot Method to Specify Lattice Parameters. Ibn Al-Haitham J Pure Appl Sci. 2023;36(1):123-129. https://doi.org/10.30526/36.1.2891.
25. Abdul-Jabbar SS, Harbbi K. Studying the relationship between the number of unit cells and the dislocation density of a crystal through the x-ray diffraction pattern of barium oxide nanoparticles. AIP Conf Proc, AIP Publishing. 2023;3018(1). https://doi.org/10.1063/5.0172073.
26. Abbas SB, Harbbi KH. Elimination of the broadening in X-ray diffraction lines profile for nanoparticles by using the analysis of diffraction lines method. AIP Conf Proc., AIP Publishing. 2022;2386(1). https://doi.org/10.1063/5.0067983.
27. Harbi KH, Abd AN. Preparation and characterization of copper oxide by adding turmeric powder. J Phys Conf Ser. IOP Publishing. 2021;1879(3):032084. https://DOI.10.1088/1742-6596/1879/3/032084.
28. Deb AK, Chatterjee P. Estimation of lattice strain in alumina-zirconia nanocomposites by X-ray diffraction peak profile analysis. J Theor Appl Phys. 2019;13:221-229. https://doi.org /10.1007/s40094-019-0338-z.
29. Scardi P, Leoni M, Delhez R. Line broadening analysis using integral breadth methods: a critical review. J Appl Crystallogr. 2004;3(37):381-390. https://doi.org/10.1107/S0021889804004583.
30. Epp J. X-ray diffraction (XRD) techniques for materials characterization, in Materials characterization using nondestructive evaluation (NDE) methods. Elsevier. 2016;23(5):81–124. https://doi.org/10.1016/B978-0-08-100040-3.00004-3.